ELSEVIER

Journal of Nuclear Materials 266–269 (1999) 30–36

journal of nuclear materials

The experimental determination of the volume recombination rate in tokamak divertors

J.L. Terry [a,*], B. Lipschultz [a], X. Bonnin [a,b], C. Boswell [a], S.I. Krasheninnikov [a,c], A.Yu. Pigarov [a,c,d], B. LaBombard [a], D.A. Pappas [a], H.A. Scott [e]

[a] *Plasma Science and Fusion Center, Massachusetts Institute of Technology, 175 Albany Street, Cambridge, MA 02139, USA*
[b] *Fusion Research Center, University of Texas at Austin, Austin, TX, USA*
[c] *I.V. Kurchatov Institute of Atomic Energy, Moscow, Russian Federation*
[d] *The College of William and Mary, Williamsburg, VA, USA*
[e] *Lawrence Livermore National Laboratory, Livermore, CA, USA*

Abstract

A method for evaluating the volume recombination rate within a cold ($T_e \lesssim 1$ eV), relatively dense ($n_e \gtrsim 1 \times 10^{21}$ m^{-3}) plasma is described. These conditions often exist in the detached divertor plasmas of the Alcator C-Mod Tokamak. Temperatures $\lesssim 1$ eV are measured spectroscopically. Densities in the 0.4×10^{21}–2.5×10^{21} m^{-3} range are measured using the Stark-broadened D^0 Balmer series lines. D^0 line emissions in both the Lyman and Balmer series show that the D^0 excited state populations ($n \gtrsim 3$) in the recombining regions are close to those given by the Saha–Boltzmann distribution and are essentially independent of the ground state density. The intensities of lines from these excited states are related to the recombination rate. The number of recombinations per D^0 photon is a function of opacity of the Lyman series lines, T_e and n_e. Determinations of the recombination rates corresponding to the line intensities are made by using a collisional radiative model describing the level populations, ionization and recombination of D^0 and a model which accounts for the radiation transfer of the Lyman lines. The effects of the trapping of Lyman photons on the 'recombinations per photon' curves have been calculated using both modelling which considers only spatial diffusion of the photons and modelling by a radiative transfer code which calculates photon transport in space and frequency. Subject to imperfect knowledge of the 2D profiles of opacity and temperature, total recombination rates in the detached divertor plasma are determined. In the Alcator C-Mod divertor region, volume recombination can be a significant sink for ions under detached conditions.

Keywords: Recombination; Atomic physics; Hydrogen; Detached plasmas; Alcator C-Mod

1. Introduction

Volume recombination is the process by which ions and electrons recombine within the plasma to form atoms. This is observed in the divertors of most tokamaks – Alcator C-Mod [1–3], ASDEX-Upgrade [4], DIII-D [5] and JET [6,7]. Even before the experimental observations of volume recombination, computer modelling of detached, low-temperature divertor plasmas [8–13] had shown the importance of recombination and in many cases motivated the experimental investigations. The importance of volume recombination derives from the desire to understand, among other things, (1) the phenomenon of divertor detachment [14] and (2) the particle sources and sinks in the divertor. For example, the large loss in ion current to the divertor plates which occurs at detachment could be due to a decreased ionization source [15], an increased volume recombination, an increased ion-neutral friction or any combination of these. In addition, knowledge of the spatial distribution of the particle sources and sinks is crucial to the divertor modelling, since the distribution of sources and sinks

* Corresponding author. Tel.: +1-617 253 8637; fax: +1-617 253 0627; e-mail: terry@psfc.mit.edu

0022-3115/99/$ – see front matter
PII: S0022-3115(98)00812-5

can drive flows which affect particle transport. Thus, quantitative determination of the magnitude and spatial distribution of the recombination sink is desired. The experimental observations have shown a link between recombination and detachment [2,6], and on Alcator C-Mod the recombination rate has been shown to be a significant ion sink in some circumstances. However, closer quantitative examination of the rates and the role of recombination is both warranted and on-going [15,16]. It is the purpose of this paper to describe the necessary measurements and modelling of the atomic processes which allow a more quantitative determination of the recombination rate.

In Ref. [1], the quantitative link between the spectral intensities of the D^0 lines and the recombination rate was pointed out, but the effects of opacity were not included in the analysis. The concept of 'recombinations per photon', an extension of the 'ionizations per photon' concept used in Ref. [17], was introduced in Ref. [2]. The importance of opacity has been pointed out by Post [18] and others, and its effect on the recombination rates was modelled in Refs. [3,17,19]. The sensitivity of the ionization balance to the plasma parameters which determine it – T_e, n_e and opacity of the partially ionized plasma to the D^0 Lyman lines – is shown in Fig. 1 for cases with no particle transport. At low densities ($n_e + N^0 = 10^{16}$ m^{-3}, shown by the dot–dashed curves) single-step ionization competes against radiative recombination. The dashed curves illustrate the case at divertor-like densities ($n_e + N^0 = 10^{21}$ m^{-3}), but where the effects of radiation transfer are neglected (therefore a non-physical case). Since the increased three-body recombination occurring at the higher density is outweighed by the increase in multi-step ionization, the temperature at which $n_e = N^0$ decreases. The solid lines show that the inclusion of radiative transfer further decreases the temperature at which $n_e = N^0$. This occurs because the Lyman series photons (especially Ly_α), emitted in the recombination process, can be absorbed by the neutrals in the volume, which can then be collisionally ionized before re-emitting the photon. This photon trapping decreases the effective recombination rate. It also greatly complicates both the experimental determination of the recombination rate and the modelling of the entire problem because the radiation transfer makes the problem both non-linear and non-local. Electron temperature is also an important quantity in the determination of the rate, as emphasized in Fig. 1. Finally, the electron density influences the recombination rate (both directly and through the opacity), and therefore must also be known or estimated.

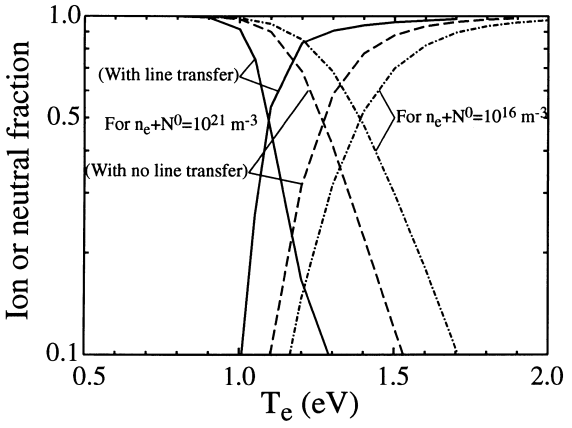

Fig. 1. The three pairs of curves show the ion and neutral fraction vs T_e in the absence of particle transport. The monotonically decreasing (increasing) curves show the neutral (ion) fraction. The dot–dashed curves illustrate the low density case. The dashed curves show the balance at divertor-like densities, but excluding opacity effects. The solid curves show the same case including the effects of opacity.

It is useful at this point to define what is meant by the 'effective recombination rate', the desired quantity. In these non-LTE plasmas the D^0 ground state is both much longer lived than the excited states, and its population density is much greater than those of the excited states. For this reason the effective recombination rate is the volume-averaged rate at which the ground state is populated by recombination. Most recombinations occur into excited states initially, and reach the ground state only after radiative or collisional decay. Thus, a recombination event is included in the 'effective' rate only after (1) a ground state atom results, and (2) any Lyman photon which was emitted in the process has escaped.

It is important to point out that the following method for determining the recombination rate applies to the volume recombination occurring as three-body and radiative recombination. It does not address another potentially important recombination process, molecular activated recombination (MAR) [20]. For details about MAR see Refs. [3,20–22].

2. Measurements of emissivities, T_e and n_e

A cross-section of the closed Alcator C-Mod divertor is shown in Fig. 2. The divertor is viewed nearly tangentially by a TV camera filtered for D_γ ($n = 5 \rightarrow 2$, where n is the principal quantum number) and by a number of spatially resolving spectrometer chords. The TV image of D_γ emission in the divertor region has been inverted (assuming toroidal symmetry) [23] to yield time-resolved 2D profiles of D_γ emissivity on a 0.01 m × 0.01 m grid. One such profile, at a time when the divertor is detached, is shown in Fig. 2. One of the many spectrometer views, in this case one which is scannable shot-to-shot, is also shown in Fig. 2. That view is shared by a

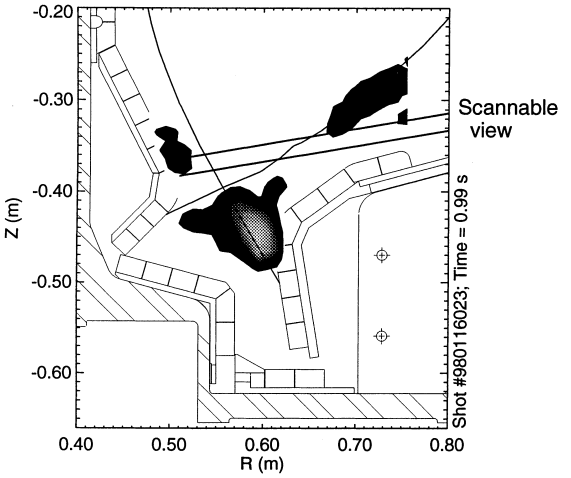

Fig. 2. A cross-section of the lower part of Alcator C-Mod, showing the measured emissivity of D_γ on a linear grayscale. Most of the emission is from the outer divertor leg. Also shown: the separatrix, the closed divertor and the scannable view shared by the Lyman series spectrograph and an instrument measuring the Balmer series. Probes embedded in the divertor plates measure the ion current to the plates.

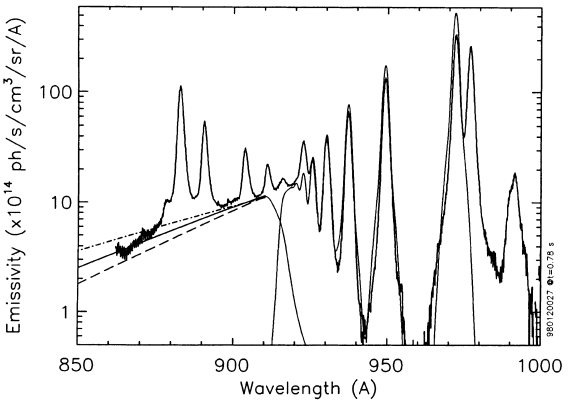

Fig. 3. The spectrum showing the $n = 4, 5, \ldots, 9 \rightarrow 1$ Lyman lines and the radiative recombination continuum emission ($\lambda \lesssim 92$ nm). The thick solid line is the experimental spectrum. The thin solid line shows the calculated line and continuum emission from a $T_e = 0.6$ eV, $n_e = 1.23 \times 10^{21}$ m^{-3} region which is 2 cm thick. The dashed line is the continuum prediction for $T_e = 0.5$ eV; the dot–dashed line is the prediction for $T_e = 0.8$ eV.

grazing incidence spectrometer, capable of measuring the D^0 Lyman series, and by an optical fibre which is coupled either to a visible spectrometer or to an interference-filtered PM tube [24]. A typical spectrum showing the Lyman series lines ($n = 4, 5, \ldots, 9 \rightarrow 1$) merging smoothly into the radiative-recombination continuum emission (corresponding to the process $e + D^+ \rightarrow D^0_{n=1} + h\nu$) is shown in Fig. 3. The spectrum of the continuum emission is essentially a measure of the electron distribution function, since $I_{cont} \propto \exp(-h\nu/T_e)$, where T_e is the emission-weighted-average temperature in the region giving rise to the emission. At low T_e the shape of the continuum spectrum is very sensitive to temperature, since $h\nu \sim 13.6$–15 eV. The best fit to the spectrum is shown in Fig. 3, with $T_e = 0.6$ eV, a temperature which is typical from spectra measured along chords viewing C-Mod's detached inner divertor. Also shown in Fig. 3 are the predicted spectral shapes for $T_e = 0.5$ and 0.8 eV, both of which depart noticeably from the measured spectrum and show the strong dependence on temperature. In addition, the D^0 line spectrum (also shown in Fig. 3) is one for which the upper levels of the lines are populated by volume recombination of free electrons and ions. The scaling of line intensity with n is quite different, depending upon whether the levels are populated by recombination or by electron impact excitation from the ground state, the other population process. The experimental spectra (both Lyman and Balmer series) for chords viewing the divertor region all typically reflect populations (for $n \gtrsim 4$) which are characteristic of recombination. This means that the populations of the levels with $n \gtrsim 4$ are essentially independent of the D^0 ground state density and that profiles of D_γ emissivity can be used to construct 2D profiles of the volume recombination rate.

The Lyman series spectrum predicted for a 0.6 eV temperature is also shown in Fig. 3 (after convolution with the spectrometer's 0.18 nm FWHM instrumental function). For the highest-n levels, the predicted line intensities agree with those measured. However, for lines from lower n levels, the predicted intensities are greater than measured. This departure between the experiment and the prediction is believed to be due to opacity, which will be discussed later. Nonetheless, the agreement in the intensities for the lines arising from the high-n levels allows for a related method of T_e measurement, which mollifies, to some extent, the fact that full spatial coverage of the divertor is not available on C-Mod by vacuum ultra-violet spectrometers. Thus, the intensity scalings of the high-n Balmer series lines, which are measured with far more extensive spatial coverage, also yield reliable values of T_e. This measurement, using the high-n Balmer series lines, is discussed in Refs. [25,26].

The electron density (weighted by $n_e \times n_i$ along the line-of-sight) can also be measured spectroscopically, using Stark-broadened Balmer lines [27]. For example, the FWHM of the $n = 8 \rightarrow 2$ line is given [28] by $\Delta\lambda_{FWHM}$ (in nm) $= 7.08 \times 10^{-15} \times n_e^{2/3}$ (n_e in m^{-3}). Densities as low as $\sim 2 \times 10^{20}$ m^{-3} can be measured, and densities as high as $\sim 2.5 \times 10^{21}$ m^{-3} have been observed in C-Mod. Values of 1.5×10^{21} m^{-3} are typical in Alcator C-Mod detached divertor plasmas.

3. Recombinations per photon

Knowledge of the local temperature, density and opacity is, in principle, enough to determine the recombination rate by evaluating directly the recombination rate coefficient, $\alpha_{\rm eff}^{\rm rec}$. However, the recombination rate coefficient, in both the optically thick and optically thin limit, is a strong function of temperature [18]. Evaluated at $n_e \sim 10^{21}$ m^{-3} with T_e in the 0.7–1.0 eV range, $(1/\alpha)\partial\alpha/\partial T_e$ varies between $\sim -5$and -3 eV^{-1}. Thus, evaluation of the recombination rate using the appropriate rate coefficient after measurement of the temperature and density requires an extremely accurate T_e measurement. The determination of the rate is made less sensitive to the accuracy of the temperature measurement by measuring the photons which are emitted in and act as 'monitors' of the recombination process. This is one of the advantages of the recombinations per photon concept. Calculated curves giving the number of recombinations per D_γ photon, (R_{D_γ}), in a plasma of $n_e = 10^{21}$ m^{-3} are shown in Fig. 4. It is seen that for D_γ, $(1/R_{D_\gamma})\partial R_{D_\gamma}/\partial T_e \sim -2.5$ to -1 eV^{-1} over the same 0.7–1.0 eV range, indicating a T_e sensitivity which is weaker than that for the recombination rate coefficient, $\alpha_{\rm eff}^{\rm rec}$. Thus, it is through these recombination per photon curves that the spatially resolved measurements of the Balmer (or Lyman) line intensities can be related to the effective recombination rates.

Calculation of the recombination per photon curves involves (1) the use of a Collisional-Radiative (CR) model for determination of the excited state population densities, and (2) a model for the radiative transfer of the D^0 emission. In the optically thin case, the number of recombinations per D_γ photon is

$$R_{D_\gamma}(T_e, n_e, \tau(\lambda) = 0) = \frac{\alpha_{\rm eff}^{\rm rec} n_e n_i}{A_{5\to 2} n_5}, \quad (1)$$

where $\tau(\lambda)$ indicates the opacity dependence, $A_{5\to 2}$ is the transition probability and n_5 is the population density of the $n = 5$ level. This quantity is shown in Fig. 4 for $n_e = 10^{21}$ m^{-3} as the solid line. For this calculation, the CR model used was the Collisional Radiative Atomic and Molecular Data code (CRAMD) [20] which uses the semi-empirical rates from Ref. [29], modified to account for the effects of statistical plasma microfields [30]. The results agree with those using the CR models of Refs. [17,31,32]. Although it is not shown in Fig. 4, there is a density dependence to the recombinations per photon curves. (There is a much stronger density dependence to the actual recombination rate.) Roughly, the recombinations per photon scale as $\sqrt{n_e}$, i.e. if there are two recombinations per photon at $n_e = 1 \times 10^{21}$ m^{-3}, there are about three recombinations per photon at $n_e = 2 \times 10^{21}$ m^{-3}.

Curves giving the number of recombinations per photon have also been calculated using the radiation transfer code CRETIN [33]. In order to compare results for the optically thin case, CRETIN was run under the condition that the neutral density times the characteristic size of the recombining region along the line-of-sight, ΔL, was low and the trapping of the Lyman lines was negligible. This result is shown as the diamonds in Fig. 4. Since very similar CR rates were used in CRETIN, good agreement with the other results is expected and observed. However, the CRETIN result also shows that, in order for the plasma to be optically thin, $N^0\Delta L$ must be $\lesssim 10^{17}$ m^{-2}, a condition which is extremely unlikely in tokamak divertors (where $\Delta L \gtrsim 0.02$ m) if the measured temperatures are $\lesssim 1.5$ eV. Very fast neutral transport would be required to keep $N^0/n_e \lesssim 5 \times 10^{-3}$ at the 0.5–1 eV temperatures measured in C-Mod. Thus, it is expected that opacity and radiative transfer play a significant role in the ionization balance in the divertor.

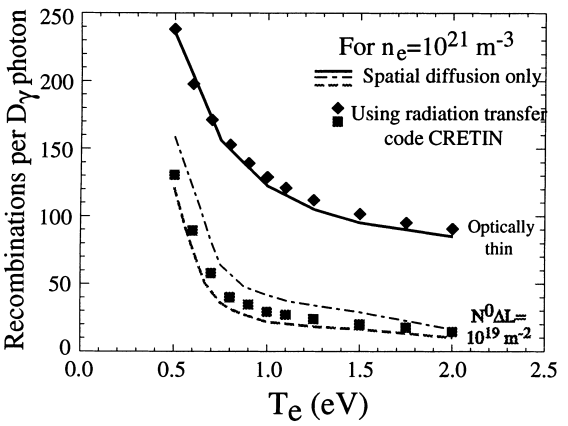

Fig. 4. The number of effective recombinations per D_γ photon in an optically thin limit (solid line and diamonds), and for two cases in which $Ly_{\alpha,\beta}$ are optically thick. The thick, dashed curve and the closed squares show the results for $N^0\Delta L = 1 \times 10^{19}$ m^{-2} using escape factor model and CRETIN, respectively. The thin, dot–dashed curve shows the case for $N^0\Delta L = 2 \times 10^{18}$ m^{-2}.

4. Opacity

The implication that opacity is important is born out of experiments. Observations that the Ly_β line is partially trapped in the divertor plasma have been made on both JET [34] and Alcator C-Mod [2,3]. Both experiments compared the time histories of the Ly_β and D_α lines when viewed along essentially identical lines-of-sight. (See the "Scannable view" shown in Fig. 2.) Since both lines arise from the same upper state, the ratio of their brightnesses is known and constant unless Ly_β is trapped or scattered before it reaches the detector. These plasmas are transparent to D_α. In Alcator C-Mod the

Ly_β/D_α ratio has been observed [3] to drop to $\sim 25\%$ of its optically thin value. Typically the ratio decreases with increasing D_α brightness. The ratio also varies somewhat depending upon the viewing geometry, as might be expected. If Ly_β is trapped, then Ly_α is predicted to be even more trapped. It should be possible to use the Ly_β/D_α ratio in combination with modelling of the radiation transfer to determine the opacity of the Lyman series along a given line-of-sight. However, it may require a full 2D treatment of the divertor since the radiation field depends upon emission at points outside the field-of-view. While this should be possible with the CRETIN code, it remains a goal at this time.

Significant progress can be made on the problem of determining the recombination rate by treating a much simpler 1D problem. This has been done in two ways, first by modelling photon diffusion in a uniform volume, and second, by modelling photon transport in both space and frequency using the CRETIN code. (In both cases T_i was taken to be equal to T_e, and both Doppler and Stark broadening were included.) For the spatial-diffusion-only treatment, CRAMD was modified to include a model for photon transport through a cylinder of uniform temperature and density with a 0.02 m diameter, ΔL. Using the well-known escape factor formalism [35], the radiative transition probabilities were reduced by a factor of $C/(1+C)$, where $C = 0.33 \times (\lambda_{mfp}/\Delta L)^2$ and λ_{mfp} is the mean-free-path for photon absorption. Thus, C depends on the product $N^0\Delta L$. In the cases where the Lyman lines are not optically thin, the definition for the number of recombinations per photon, Eq. (1), is modified to reflect the fact that the effective recombination rate is no longer a local quantity, i.e.

$$R_{D_\gamma}(T_e, n_e, \tau(\lambda)) = \frac{\langle \alpha_{eff}^{rec} n_e n_i \rangle_{vol}}{E_{5\to 2}}, \qquad (2)$$

where $\langle\ \rangle_{vol}$ is a volume average and $E_{5\to 2}$ is the average D_γ photon flux escaping the plasma volume. (Of course the Balmer lines are still thin in these cases.) The result is shown by the dashed curves in Fig. 4. As expected, the recombinations per photon drop rapidly as $nN^0\Delta L$ increases to $\sim 2 \times 10^{18}$ m^{-2}. However, for larger values of $N^0\Delta L$, the recombinations per photon drop only slightly, since Ly_α is strongly trapped in the interior of the volume. Thus, the lower curves shown in Fig. 4 represent the appropriate 'optically thick' limit for these plasmas.

The results using the spatial diffusion/escape factor modelling have been compared with those calculated using the CRETIN code. In this case the volume modelled was a 0.02 m thick slab of uniform temperature and density. The results are also shown in Fig. 4 where the recombinations per photon curve calculated using CRETIN (the squares) is compared with the dashed curve. The CRETIN values are only slightly greater than those of the escape factor modelling. Since the CRETIN code models photon transport in both space and frequency, and since diffusion in frequency allows a greater number of photons to escape, the closeness of the two results may mean that the reduction in opacity brought about by frequency diffusion is partly compensated by the fact that a slab geometry is somewhat thicker than a cylindrical geometry, as modelled using CRAMD. Nonetheless, the conclusion reached using the two different models with two different (but simple) geometries is that the recombinations per photon are reduced from the optically thin values by a factor from $\sim$2 to 8, depending on T_e.

5. Recombination rate results

Ideally, the measurements and calculations described above allow accurate determination of the recombination rate by the following procedure: (1) measure the D_γ emissivity profile (as shown in Fig. 2) or measure the D_γ brightness along many chords spanning the divertor region, (2) measure T_e either using the slope of the radiative recombination continuum or by using the high-n line intensity scaling, (3) measure the Ly_β/D_α ratio along many chords spanning the divertor region and model the results using a 2D radiative transfer code like CRETIN, (4) measure the electron densities using Stark-broadened Balmer lines, and (5) multiply the D_γ emissivity by the number of recombinations per D_γ photon appropriate to the measured temperature, opacity and density. In the absence of a complete set of these measurements, a number of approximations may be made. First, it is likely that, at least for Alcator C-Mod, the optically thick recombinations per photon curves are appropriate. In other words, curves like that given by the squares in Fig. 4, but generated for different densities, can be used. Secondly, the temperatures and densities measured along a limited number of views can be used to evaluate the number of recombinations per photon. This utilizes the reduced sensitivity of the recombinations per photon (as compared to direct evaluation of the effective recombination rate coefficient). It also utilizes the advantage that the number of D_γ photons emitted can be reasonably well measured. This compensates for the imperfect knowledge of details of the T_e and n_e profiles along a given line-of-sight.

This approximate procedure has been used to evaluate the time history of the recombination rate in an Alcator C-Mod discharge in which the density was increased during the shot in order to detach the plasma from the divertor plates. The emissivities measured using the D_γ-filtered TV view (Fig. 2) were used, as were the recombination per D_γ photon curves (Fig. 4) as calculated by CRETIN. The total recombination rate is calculated from

$$\int_{\text{vol}} E_{5\to2} R(T_e, n_e, \tau)\ \mathrm{d}v, \tag{3}$$

where in this very simplified treatment, $R(T_e, n_e, \tau)$ is taken as constant over the regions of non-zero D_γ emissivity. A more complete treatment using this method, using additional views and a varying R, is given in Ref. [15]. The result is shown in Fig. 5, where the recombination rate is shown along with the total ion current to the divertor plates. The ion current is the other sink for ions and is measured by two probe arrays mounted in the plates. A slow detachment begins at ~0.7 s, when the ion current starts to decrease. The thin solid line corresponds to the result using $R_{D_\gamma} \sim 35$, the optically thick value calculated by the CRETIN modelling for $T_e = 0.9$ eV, $n_e = 10^{21}$ m^{-3}. The thick line shows the result using $R \sim 130$ recombinations per D_γ, the CRETIN calculated value at 0.5 eV. Although the optically thick curves were used in this determination, it is noteworthy that spatial inhomogeneities in N^0 tend to make the plasma less thick, since thinner regions allow more Lyman photons to escape. This effect would increase the recombination sink shown in Fig. 5.

It is clear that in the fully detached state, the ion sink from volume recombination is greater than or approximately equal to ion current to the plate and recombination can be a significant sink for ions. However, it is also likely that the loss of ion current which occurs from 0.7 to 1.0 s has not been compensated by an increase in volume recombination. This issue is discussed in detail in Ref. [15], where more carefully determined time histories of T_e and n_e were used in the analysis.

Measurement of the 2D emissivity profiles along with the recombination per photon curves also allows diagnosis of the spatial structure of the recombining region. For the discharge shown in Fig. 5, it is observed that, as detachment occurs, the recombination moves away from the plate and is distributed mostly along the outer leg of the separatrix between the plate and the X-point, as shown in Fig. 2.

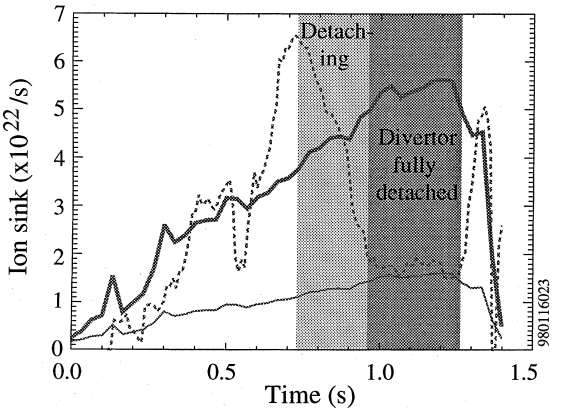

Fig. 5. Time histories of the two ions sinks: the total ion current to the plates (dashed), and the volume recombination sink (solid). The thick and thin solid lines correspond to the use of different R_{D_γ} values in the determination of the recombination sink. After ~0.7 s, plasma detachment from the outer divertor plate begins and reaches a fully detached state just before 1.0 s.

6. Discussion and summary

The purpose of this paper is to describe a method by which the volume recombination rate can be evaluated using experimental measurements. An additional goal is to detail some of the difficulties in this evaluation. It should be clear that radiative transfer effects, although necessary in the analysis, complicate the evaluation and the interpretation of the measurements. The modelling in simplified geometry, with uniform temperature and density, which has been done for this work, is only a first step to understanding the problem of sources and sinks in these kinds of divertor plasmas. A more accurate treatment of Stark broadening and Zeeman splitting can be used in the radiation transfer modelling. 1D and 2D modelling is possible using CRETIN, but eventually radiative transfer should be coupled to codes like UEDGE or B2-EIRENE which describe the neutral and plasma processes in the plasma divertor/edge. The radiative transfer problem can be studied experimentally with good measurements of the Lyman and Balmer spectra along the same view.

Other uncertainties are introduced in this method by the assignment of a single T_e and n_e to a single region viewed by each chordal measurement. In fact, each viewing chord passes through non-uniform plasma, and the effects of this are difficult to quantify. Regions of $T_e \gtrsim 3$ eV or $n_e \lesssim 10^{20}$ m^{-3} (for C-Mod) are probably not important, since there is essentially no recombination there and since those regions contribute little to the D^0 spectrum. It is the transition region from the plasma whose parameters are measured, i.e. ~0.7 eV, 10^{21} m^{-3}, to the hotter, less dense plasma, which complicate the analysis and whose effects should be estimated. The transition region is especially important in trying to understand the $Ly_{\alpha,\beta}$ emissions which come both from the edges of the optically thick regions and from the hotter transition region where ionization is occurring. Refs. [3,30] analyzed features of the D^0 spectrum by considering emission contributions from both a 'cold' and 'hot' (~3 eV) region within the field-of-view. These improvements also move in the direction of a full 2D description of the emission. Considering the approximations used here in order to deal with these complications, it is estimated that the experimental determinations of the recombination rate are uncertain by about a factor of 2. This uncertainty must be reduced, since, as evidenced by the curves in Fig. 5, the

deduced recombination rate is neither negligible nor overwhelming ion sink in the divertor for the cases of interest.

In summary, measurements of the plasma parameters in regions of recombining plasma show that typically $T_e \lesssim 1$ eV and $n_e \gtrsim 1.5 \times 10^{21}$ m^{-3} in the Alcator C-Mod divertor under detached conditions. Other measurements show that at least the Ly_α and Ly_β lines are significantly trapped in these plasmas. It has been described how D_γ emissivity profiles can be used in conjunction with curves relating the number of recombinations to the number of emitted D_γ photons to determine the rate of volume recombination. The recombinations per photon values are functions of temperature and Lyman line opacity, and weakly dependent on electron density. The effects of opacity upon the effective recombination rate have been calculated in two ways: (1) considering spatial diffusion of the photons out of a uniform volume, and (2) using the non-LTE radiative transfer code CRETIN which includes both spatial and spectral diffusion. Both results show that radiative transfer is important in describing the ionization/recombination balance under conditions found in the C-Mod divertor. The ion sink due to volume recombination, evaluated using these measurements and this formalism, is shown to be significant in some detached discharges.

Acknowledgements

This work is supported by the US Department of Energy under the contract # DE-AC02-78ET51013 and under the grant #DE-FG02-910ER-54109. The authors thank Alan Wan of LLNL for his help in procuring the CRETIN code.

References

[1] D. Lumma, J. Terry, B. Lipschultz, Phys. Plasmas 4 (1997) 2555.
[2] J. Terry, B. Lipschultz, B. LaBombard, D. Pappas, in: Proceedings of the 24th European Phys. Soc. Conf. on Contr. Fus. and Plasma Phys. Part II, European Physical Society, vol. 21A, Petit-Lancy, 1997, p. 573 .
[3] J. Terry et al., Phys. Plasmas 5 (1998) 1759.
[4] B. Napiontek et al., in: Proceedings of the 24th European Phys. Soc. Conf. on Contr. Fus. and Plasma Phys. Part IV, European Physical Society, vol. 21A, Petit-Lancy, 1997, p. 1413.
[5] R. Isler et al., Phys. Plasmas 4 (1997) 2989.
[6] G. McCracken et al., Nucl. Fusion 38 (1998) 619.
[7] G. McCracken et al., these Proceedings.
[8] A. Loarte, J. Nucl. Mater. 241–243 (1997) 118.
[9] F. Wising, D. Knoll, S. Krasheninnikov, T. Rognlien, D. Sigmar, Contrib. Plasma Phys. 36 (1996) 136.
[10] G. Porter et al., Phys. Plasmas 3 (1996) 1967.
[11] K. Borrass, D. Coster, D. Reiter, R. Schneider, J. Nucl. Mater. 241–243 (1997) 250.
[12] S. Krasheninnikov et al., Phys. Plasmas 4 (1997) 1638.
[13] M. Fenstermacher et al., Phys. Plasmas 4 (1997) 1761.
[14] G. Matthews, J. Nucl. Mater. 220–222 (1995) 104.
[15] B. Lipschultz et al., these Proceedings.
[16] S. Krasheninnikov et al., these Proceedings.
[17] L. Johnson, E. Hinnov, J. Quant. Spectrosc. Radiat. Transfer 13 (1973) 333.
[18] D. Post, J. Nucl. Mater. 220–222 (1995) 143.
[19] K. Behringer, The influence of opacity on hydrogen line emission and ionisation balance in high density divertor plasmas, Max Plank Inst. fur Plasmaphysik, Report IPP 10/5, unpublished.
[20] A. Pigarov, S. Krashenninikov, Phys. Lett. A 222 (1996) 251.
[21] S. Krasheninnikov, A. Pigarov, T. Soboleva, D. Sigmar, J. Nucl. Mater. 241–243 (1997) 283.
[22] N. Ezumi et al., in: Proceedings of the 24th European Phys. Soc. Conf. on Contr. Fus. and Plasma Phys., Part III, European Physical Society, vol 21A, Petit-Lancy, 1997, p. 1225.
[23] A. Allen, Capture, storage, and analysis of video images on the Alcator C-Mod Tokamak, M.I.T. M.S. Thesis, PSFC Report PSFC/RR-97-1, 1997.
[24] H. Ohkawa, Determination of the spectral sensitivity of a VUV, grazing incidence spectrograph, M.I.T. M.S. Thesis, PSFC Report PSFC/RR-97-11, 1997.
[25] H. Griem, Spectral Line Broadening by Plasmas, Academic Press, New York and London, 1974.
[26] B. Lipschultz et al., Ultrahigh densities and volume recombination inside the separatrix of the Alcator C-Mod Tokamak, Phys. Rev. Lett. 81 (1998) 1007.
[27] B. Welch et al., Phys. Plasmas 2 (1995) 4246.
[28] R. Bengtson, J. Tannich, P. Kepple, Phys. Rev. A 1 (1970) 532.
[29] L. Johnson, Ap. J. 174 (1972) 227.
[30] A. Pigarov, J. Terry, B. Lipschultz, Study of the discrete-to-continuum transition in a Balmer spectrum from Alcator C-Mod divertor plasmas, Plasma Phys. Controlled Fusion, 1999, in press.
[31] T. Fujimoto, S. Miyachi, K. Sawada, Nucl. Fus. 28 (1988) 1255.
[32] H. Drawin, F. Emard, Physica C 85 (1977) 333.
[33] H. Scott, R. Mayle, Appl. Phys. B 58 (1994) 35.
[34] T. Lovegrove et al., in: Proceedings of the 22nd European Phys. Soc. Conf. on Contr. Fus. and Plasma Phys., Part III, European Physical Society, vol 19C, Petit-Lancy, 1995, p. 301.
[35] F. Irons, J. Quant. Spectrosc. Radiat. Transfer 43 (1990) 107.